Editors' Suggestion

Electric field controllable high-spin $SrRuO_3$ driven by a solid ionic junction

Jingdi Lu,[1,*] Liang Si,[2,3,*] Xiefei Yao,[1,*] Chengfeng Tian,[1,*] Jing Wang,[4,5,*] Qinghua Zhang,[6,*] Zhengxun Lai,[7] Iftikhar Ahmed Malik,[1] Xin Liu,[1] Peiheng Jiang,[2] Kejia Zhu,[6] Youguo Shi,[6] Zhenlin Luo,[8] Lin Gu,[6] Karsten Held,[3] Wenbo Mi,[7] Zhicheng Zhong,[2,†] Ce-Wen Nan,[4] and Jinxing Zhang[1,‡]

[1]*Department of Physics, Beijing Normal University, 100875 Beijing, China*

[2]*Key Laboratory of Magnetic Materials and Devices & Zhejiang Province Key Laboratory of Magnetic Materials and Application Technology, Ningbo Institute of Materials Technology and Engineering (NIMTE), Chinese Academy of Sciences, Ningbo 315201, China*

[3]*Institut für Festkörperphysik, TU Wien, Wiedner Hauptstraße 8-10, 1040 Vienna, Austria*

[4]*School of Materials Science and Engineering, Tsinghua University, 100084 Beijing, China*

[5]*Advanced Research Institute of Multidisciplinary Science, Beijing Institute of Technology, Beijing 100081, China*

[6]*Institute of Physics, Chinese Academy of Science, 100190 Beijing, China*

[7]*Tianjin Key Laboratory of Low Dimensional Materials Physics and Preparation Technology, School of Science, Tianjin University, Tianjin 300354, China*

[8]*Department of Physics, National Synchrotron Radiation Laboratory, CAS Key Laboratory of Materials for Energy Conversion, University of Science and Technology of China, Hefei 230026, China*

(Received 10 March 2020; revised manuscript received 12 May 2020; accepted 13 May 2020; published 1 June 2020)

Controlling magnetism and spin structures in strongly correlated systems by using electric fields is of fundamental importance but challenging. Here, a high-spin ruthenate phase is achieved via a solid ionic chemical junction at the $SrRuO_3/SrTiO_3$ interface with distinct formation energies and diffusion barriers of oxygen vacancies, an analog to electronic band alignment in the semiconductor heterojunction. Oxygen vacancies trapped within this interfacial $SrRuO_3$ reconstruct the Ru-4*d* electronic structure and orbital occupancy, leading to an enhanced magnetic moment. Furthermore, this emergent interfacial magnetic phase can be switched reversibly by electric-field-rectifying oxygen migration in a solid-state ionic gating device, providing a framework for the atomic design of functionalities in strongly correlated oxides using a method of solid chemistry.

DOI: 10.1103/PhysRevB.101.214401

I. INTRODUCTION

Controlling magnetism and low-dimensional spin textures in strongly correlated systems by electric fields has a widespread potential for many information processing applications requiring low-power consumption [1–4]. Over past decades, the spin degree of freedom has been effectively controlled by electric fields in magnetoelectrics and multiferroic heterostructures [5–11]. However, the control of these ferroic orderings and direct characterization of their coupled behaviors by using advanced approaches are still fundamentally challenging [1,3]. Therefore, it is desirable to design new correlated electron systems with atomic precision by engineering material chemistries and architectures [3]. Transition-metal oxides (TMOs) with strong *d*-electron correlations and spin-orbit coupling (SOC) may provide an effective platform towards emergent magnetism with controllable spin textures [12–20].

$SrRuO_3$ (SRO) is a 4*d* TMO with a coexistence of SOC and itinerant ferromagnetism [21], leading to a large variety of physical behaviors which have been experimentally observed, such as high-spin states driven by crystal orientations [22–24], magnetic skyrmions due to the broken symmetry [25–28], and metal-insulator transition [29–31], etc. More importantly, emergent physical behaviors have been theoretically proposed in SRO recently [13,15,32,33], triggering broad attention to discover the potential quantum states in this material. Among these theories, heavy electron doping in SRO seems to be effective to further enhance magnetism and change electronic structure [15], which is, however, experimentally challenging in this oxide with a metallic ground state. Although a high concentration of the oxygen vacancy (v_O) is equivalent to electron doping, it is hard to be achieved in bulk SRO. This gives a strong impetus to explore an alternative pathway to build upon the above physical scenario. Inspired by electrons rectifying at solid-state junctions, such as the well-known diode at *p-n* junctions [34], a solid ionic chemical junction may be used to rectify v_O by using its chemical discontinuity across the interface [35].

II. EPITAXIAL SRO THIN FILMS WITH MONOCLINIC STRUCTURE

Atomically flat SRO thin films with accurate thicknesses of 5, 10, 30, and 50 uc (where uc is the unit cell) were grown on (001)-oriented $SrTiO_3$ (STO) substrates with TiO_2 termination by pulsed laser deposition with *in-situ* reflection

*These authors contributed equally to this work.
†zhong@nimte.ac.cn
‡jxzhang@bnu.edu.cn

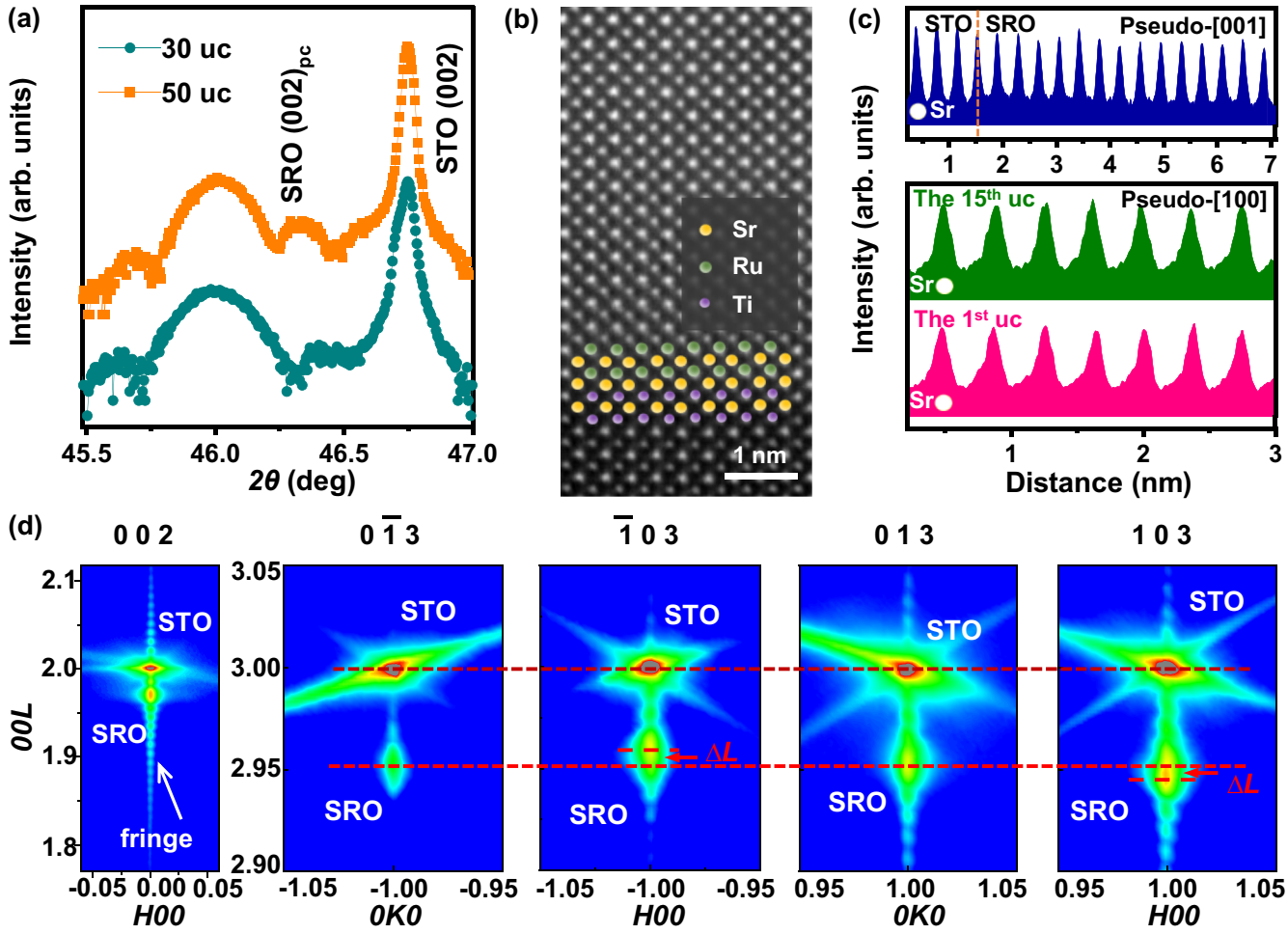

FIG. 1. High-quality monoclinic SRO thin films without strain relaxation. (a) The θ-2θ SXRD spectra for (002)-oriented sets of peaks. The SRO thin film is the pseudocubic phase (pc). (b) High-resolution cross-section STEM image of the 50-uc SRO thin film. (c) Line profiles of the SrO layers below 15 uc at the pseudo-[001] orientation (top panel) and line profiles of the SrO layers for the first uc and the 15th uc of the SRO thin film (bottom panel). (d) RSM for the 50-uc SRO on STO (001) around (002) and {103} STO Bragg reflection in the reciprocal lattice units of STO with the thickness fringes. The dissimilar values (ΔL) indicate the monoclinic structure where cell parameters measured for the 50-uc SRO thin film are $a_{pc} = 3.905$, $b_{pc} = 3.905$, $c_{pc} = 3.967$ Å, $\alpha = 90°$, $\beta = 89.82°$, and $\gamma = 90°$.

high-energy electron diffraction. Through a synchrotron-based x-ray-diffraction (SXRD) study, a set of (002)-oriented peaks in Fig. 1(a) reveals SRO thin films with a c-axis lattice constant of 3.967 Å (thickness up to 50 uc). The epitaxial growth of SRO thin films is shown in Fig. S1 of the Supplemental Material [36]. High-resolution scanning transmission electron microscopy (STEM) in Fig. 1(b) indicates a high-quality and dislocation-free epitaxy for the SRO thin films. The out-of-plane and in-plane lattice structures in STEM [Fig. 1(c)] illustrate that there is an in-plane compressive strain ($\sim -0.45\%$) without any relaxation and phase separation across the whole SRO thin films, which are consistent with the results obtained from the x-ray reciprocal space mapping (RSM) [Fig. 1(d)]. The monoclinic structure of the SRO thin films [37] has been further revealed by the x-ray RSM. The details of growth and measurements can be seen in the Supplemental Material [36].

III. EMERGENT HIGH-SPIN SRO DRIVEN BY INTERFACIALLY TRAPPED OXYGEN VACANCIES

The ferromagnetic Curie temperature (T_C) was measured as a function of thickness by temperature-dependent magnetization and resistivity (M-T and R-T) [21,40]. As shown in Figs. 2(a) and 2(b), $T_C \sim 125$ K is observed for the 50-, 30-, and 10-uc SRO thin films, whereas another $T_C \sim 153$ K is observed in thin films with thicknesses of 30, 10, and 5 uc. The $T_C \sim 125$ K is ascribed to the fully strained monoclinic structure as studied previously [37,41], which is lower than the bulk orthorhombic SRO (T_C is ~160 K) [42]. The two distinct T_C values maintain in all films, although a single $T_C \sim 153$ K exists in a 5-uc SRO thin film. The thickness-dependent magnetic hysteresis loops along the pseudo-[001] axis were measured with a superconducting quantum interference device magnetometer [Fig. 2(c)]. Upon increasing the thickness

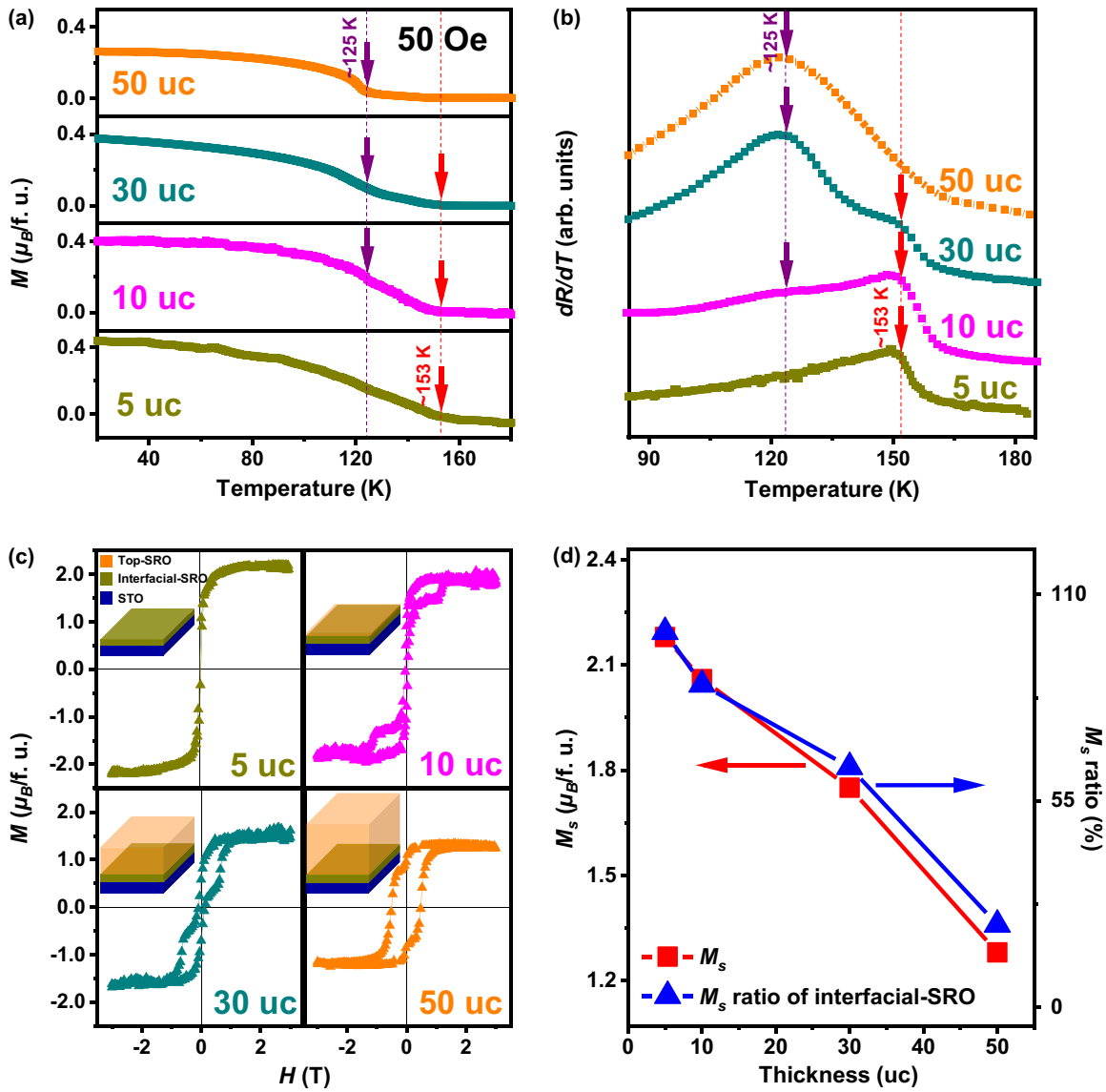

FIG. 2. Emergent interfacial magnetic phase with an enhanced magnetization. (a) Temperature-dependent magnetization (M-T curves) shows two T_C values determined by the discontinuity in dM/dT (red and purple arrows). (b) Temperature-dependent differential resistivity (dR/dT-T) at a constant magnetic field of 1 T (helpful to obtain well-defined peaks at T_C) shows that the T_C's are consistent with the ones from M-T curves, indicating that the interfacial SRO contributes to the high T_C. (c) Out-of-plane magnetic-field-dependent magnetization (M-H curves) at 10 K. The insets are the schematics of the interfacial-SRO and top-SRO phases. (d) Thickness-dependent out-of-plane M_s (red curves) and its contribution from the interfacial SRO (blue curves). As the thickness increases, the M_s decreases, which indicates that the interfacial SRO contributes to the enhancement of M_s. All the above data obtained from the SRO thin films with thicknesses of 5, 10, 30, and 50 uc.

from 5 to 10 uc, a steplike hysteresis with two coercive fields appears, which is more obvious in the 30- and 50-uc thin films. For the 5-uc SRO, the out-of-plane saturated moment (M_s) is $\sim$2.18 μ_B/formula unit (f.u.), which is higher than the one of low-spin state of SRO ($\sim$1.1$-$2.0 μ_B/f.u. in experiments and theories, 2.0 μ_B/f.u. from the full Hund's rule) [43–46]. As the thickness increases, M_s decreases to $\sim$2.06, $\sim$1.75, and $\sim$1.28 μ_B/f.u. for 10-, 30-, and 50-uc SRO, respectively, indicating that the SRO at the interface contributes to the enhancement of M_s as shown in insets of Figs. 2(c) and 2(d). The magnetic domain switching, corresponding to the hysteresis, has been characterized by using low-temperature magnetic force microscopy (MFM) at 10 K. For the 5-uc SRO, a monodomain switching occurs (Fig. S2 of the Supplemental Material [36]). However, for the SRO thin film with a thickness above 10 uc, there is a distinctive switching with two coercive fields at low/high magnetic field (Fig. S3 of the Supplemental Material [36]), which further indicates that the steplike magnetic hysteresis could be attributed to a separation of magnetic phases: interfacial SRO (high T_C/moment) and top SRO (low T_C/moment). The hysteresis behavior as a function of top-SRO thickness is simulated in Fig. S4 of the Supplemental Material [36], which is consistent with our experimental observations in Fig. 2(c). The details of measurements for magnetic/electrical characterizations are given in the Supplemental Material and Fig. S5 [36].

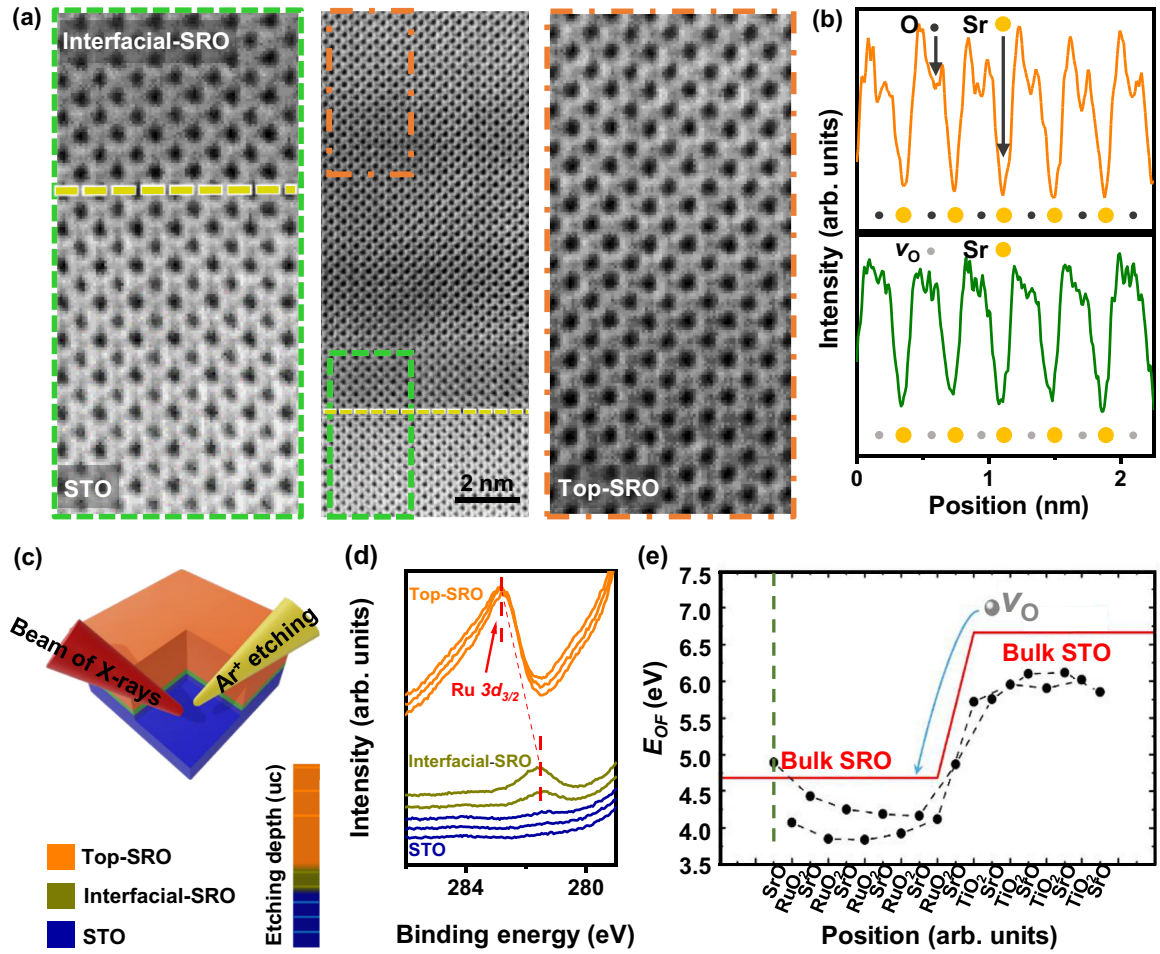

FIG. 3. Evidence of the interfacial-SRO phase driven by an ionic chemical junction. (a) Bright-field STEM of the SRO on STO. The left and right panels show the magnified bright-field STEM image as labeled by the rectangle boxes in the middle panel. (b) The corresponding line profile for the detailed atomic structure of SrO layers in the interfacial SRO (bottom panel, green curve) and top SRO (top panel, orange curve). The yellow, dark gray, and light gray dots represent the positions of Sr, O, and v_O, respectively. The shallow valleys in the orange curve represent oxygen sites, which are negligible in the green curve, indicating more v_O's located at the interface. (c) Schematic of the depth-profile XPS measurements with *in situ* Ar^+ etching. (d) Depth-profile binding energies of Ru $3d_{3/2}$ shows a dramatic change in binding energies for Ru $3d_{3/2}$. (e) Calculation of the formation energies and diffusion barriers of v_O across the SRO/STO interface. The black dots are the formation energies E_{OF} of the v_O's located at different layers across SRO/STO interface. The red lines are the bulk values of SRO and STO at $\sqrt{2}\times\sqrt{2}\times4$ dimension. The gray sphere indicates that v_O prefers to diffuse from STO into SRO and be prevented at the position of the green dashed line (diffusion length).

In these fully strained SRO thin films without lattice relaxation, slight alternation of the chemical structure at the interface may play a key role in the enhanced magnetization [47]. As seen from bright-field STEM in Figs. 3(a) and 3(b), the interfacial-SRO phase presents more v_O which is negligible in the top SRO. Depth-profiling x-ray photoelectron spectroscopy (XPS) with *in situ* etching of surface layers without damaging underlying layers [see Fig. 3(c) for the schematics] shows the valence states of Ru at various etching depths for the 50-uc SRO in Fig. 3(d). The binding energy of Ru $3d_{3/2}$ remains at ~282.82 eV whereas etching away up to 30 uc. However, it starts to dramatically decrease by ~1.3 eV when the etching depth reaches about 45 uc, indicating that Ru^{3+} appears at the interfacial SRO [48]. At all conditions, there is no change for the binding energies of Sr $3d$ from the top SRO to the interfacial SRO and then STO (see Fig. S6 of the Supplemental Material [36]). Therefore, the appearance of Ru^{3+} at the interfacial SRO is induced by the v_O based on the above analysis of STEM and XPS results [48]. The detailed measurements for chemical structures are given in the Supplemental Material [36].

The microscopic origin of this v_O-dominant interfacial-SRO phase with enhanced M_s can be understood by calculating the formation energy (E_{OF}) and the diffusion barrier (E_b) of the v_O in both SRO and STO. The E_{OF} is defined as

$$E_{OF} = E_{SC}(v_O)\text{-}E_{SC} + E(O_2)/2$$

for both SRO and STO in density functional theory (DFT). Here, $E_{SC}(v_O)$ and E_{SC} are the energies of supercells with and without a v_O, respectively, and $E(O_2)$ is the energy of a single O_2 molecule. The E_{OF} of bulk SRO is ~4.7 eV, which is ~2 eV lower than that of bulk STO, indicating that v_O prefers to be on the SRO side. Near the SRO/STO interface,

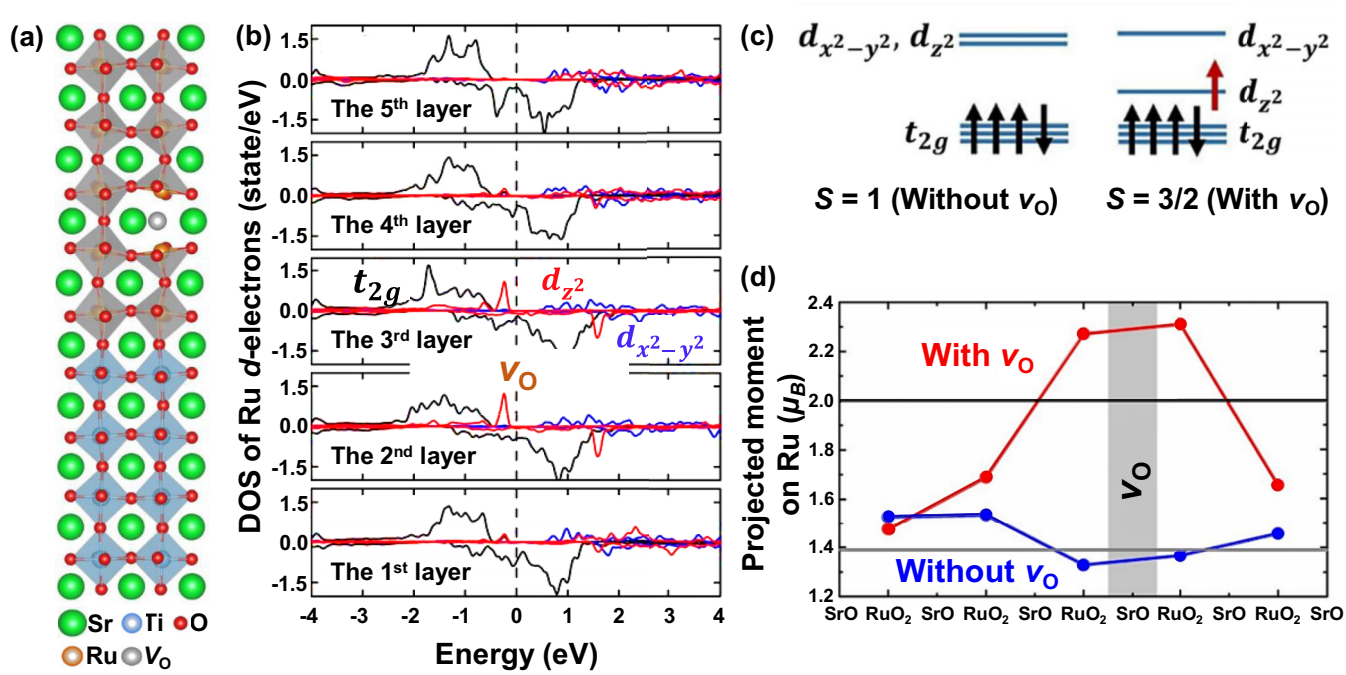

FIG. 4. Microscopic origin of the interfacial high-spin SRO. v_O-induced orbital reconstruction turns the initial $4d^4$ low-spin state ($S = 1$) into the $4d^5$ high-spin state ($S = 3/2$). In addition, the local magnetic moments of Ru sites neighboring the v_O are significantly larger than that of other Ru sites far away from v_O. Moreover, they are beyond the upper limit of low-spin states predicted by Hund's rule for Ru^{4+} ($t_{2g}^3 \uparrow, t_{2g}^1 \downarrow$, 2 μ_B/Ru), which supports the emergence of the high-spin state. (a) The crystal structure of the SRO/STO heterostructure used in calculations where four STO substrate layers and five SRO layers are constructed, and an oxygen atom is removed to model v_O. (b) DFT-resulted layer-dependent DOS of Ru d-electrons. The v_O is set in between the second and third RuO_2 layers. (c) The schematics of electronic configuration of the low-spin state without v_O and the high-spin state with v_O. (d) Projected magnetic moments on Ru atoms with (red dots) or without (blue dots) v_O. The v_O locates between the second and the third RuO_2 layers as indicated by the gray area. The black and gray lines are the upper limit of the low-spin state and the projected moment on Ru atoms in bulk SRO, respectively.

the E_{OF} of a single v_O in SRO is ~4 eV, lower than that in STO [Fig. 3(e)]). Therefore, we expect that v_O migrates into the interfacial-SRO phase when SRO is in contact with STO. In Fig. S7 of the Supplemental Material [49], we further calculated the diffusion energy barrier E_b of v_O. In SRO, E_b is ~1.4 eV, which is much higher than the one in STO (~0.6 eV). Whereas for STO, such a barrier height permits v_O diffusion, and, in SRO, it prevents v_O diffusing further into the top-SRO phase [58]. As a result, the v_O is trapped at the interfacial-SRO phase as visualized in Fig. 3(e) and forms a v_O diode in a similar way as electron diffusion in a conventional electrical diode.

For understanding the role of v_O in the enhanced M_s at the interfacial-SRO phase, we construct a SRO (5-uc)/STO (4-uc) heterostructure where one oxygen atom is removed between the second and the third RuO_2 layers to model the v_O [see Figs. 4(a) and 4(b)]. There are substantial spin and orbital reconstructions of the Ru d electrons near the v_O. The occupation of the Ru d_{z^2} orbit arises from the fact that: (i) v_O provides abundant electrons, and (ii) it breaks the neighboring RuO_6 octahedron and changes the crystal-field splitting. The latter shifts the energy of the d_{z^2} orbit down by forming bonding and antibonding states. This orbital reconstruction is pivotal for turning the $4d^4$ low-spin state ($S = 1$, ~1.5 μ_B/Ru, far away from v_O) into a $4d^5$ high-spin state ($S = 3/2$, ~2.3 μ_B/Ru, neighboring v_O) as shown in Figs. 4(c) and 4(d), being compatible with our experimental results [Fig. 2(d)]. Thus, the interfacial-SRO phase with high spin can be defined as the v_O-SRO phase. The computational details are attached in the Supplemental Material [49].

IV. ELECTRIC-FIELD CONTROL OF THE MAGNETIC PHASE TRANSITION

The interfacial high-spin SRO phase originates predominately from the v_O contributions, which could be naturally controllable in this v_O diode across the solid v_O-SRO/STO chemical junction by an electric field [59]. The temperature-dependent transport measurements with *in situ* magnetic-domain characterizations were performed in the 10-uc SRO thin film under the application of an electric field as schematically shown in Fig. 5(a). A reversible control of the v_O SRO (T_C is ~153 K) was achieved by electric-field-driven unidirectional v_O migration from SRO to STO as shown in Fig. 5(b), demonstrating that the v_O SRO with high spin can be erased and rebuilt by applying electric fields. With a magnetic bias between the coercive fields of v_O SRO and the top SRO, the "soft" v_O SRO will switch first and serve as an effective magnetic field (H_{eff}). Magnetic domain switching with and without the application of electric fields has been performed under a magnetic bias of +0.75 T, which is lower than the coercive field of the top SRO in the 10-uc film [~1 T, see Fig. 2(c)]. With the application of the electric field of +4 kV cm^{-1}, magnetic domains cannot be switched at the

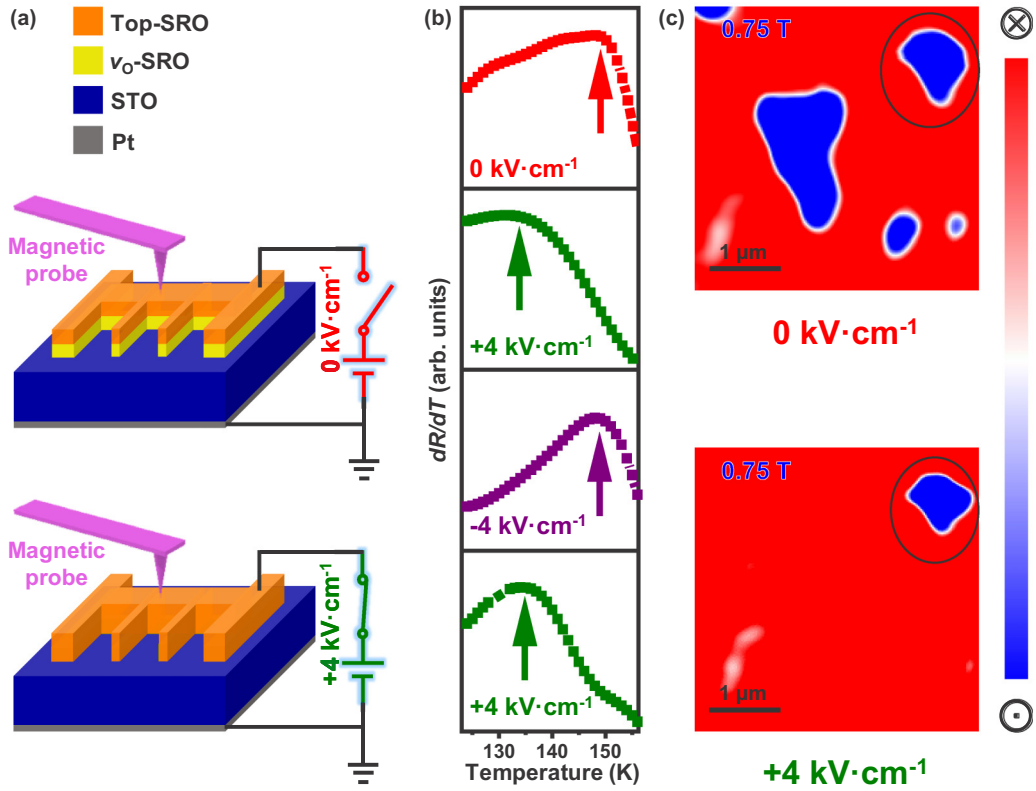

FIG. 5. Electric-field control of T_C and mesoscopic domains switching. (a) Schematics of electrical transport under an electric field with *in situ* MFM measurement in a solid-state ionic gating device. The electric fields are maintained during measurements. (b) Reversible control of T_C derived from dR/dT-T curves (the red, green, and purple arrows) due to the erasing and rebuilding of the v_O-SRO with the application of the vertical electric field of 0, +4, -4, +4 kV cm^{-1}. (c) Magnetic domain switching in top-SRO/v_O-SRO (total thickness of 10 uc) without/with the application of the electric field where the magnetic domains were captured at 10 K with/without v_O SRO. The black circles indicate that the images were captured in the same area.

same magnetic bias as the v_O SRO (namely, H_{eff}) has been erased as shown in Fig. 5(c). The details on measurements can be seen in the Supplemental Material [36].

V. CONCLUSION

To summarize, by designing an oxygen ionic chemical junction, v_O's are trapped at the interfacial-SRO phase, leading to an electronic and orbital reconstruction. As a result, a high-spin state at the v_O-SRO phase is achieved, which is reversibly switchable by an electric-field-induced oxygen migration in a solid-state ionic gating device. Furthermore, understanding of electronic and spin states in such a low-dimensional SRO phase makes this strongly correlated system a promising candidate for the further exploration and manipulation of emergent magnetism and spin structures.

ACKNOWLEDGMENTS

We gratefully acknowledge the discussions with Professor N. A. Spaldin in Materials Theory of ETH Zürich, Dr. L. Wang in the Center for Correlated Electron Systems of Institute for Basic Science, and Dr. M. Kim from the Department of Physics, Rutgers University. The work was supported by the National Key Research and Development Program of China through Contracts No. 2016YFA0302300, No. 2016YFA0300102, and No. 2017YFA0303602, the Basic Science Center Program of the NSFC under Grant No. 51788104, the National Natural Science Foundation of China (Grants No. 11974052, No. 11675179, No.11774360, and No. 11904373), the Beijing Natural Science Foundation (Grant No. Z190008), and the CAS Interdisciplinary Innovation Team. L.S. and K.H. were supported by the European Research Council (ERC) under the European Union's Seventh Framework Program (Program No. FP/2007-2013) through ERC Grant No. 306447 and by the Austrian Science Fund (FWF) through Project No. P 30997. L.S. was also funded by the China Postdoctoral Science Foundation (Grant No. 2019M662122). Beam time from APS 33BM and SSRF 14B and the 3315 Program of Ningbo are appreciated. Calculations have been performed on the Supercomputing Center at NIMTE CAS and Vienna Scientific Clusters (VSC).

J.Z. and Z.Z conceived the experiments and prepared the paper. X.Y. and C.T. fabricated the thin films. K.Z. and Y.S. prepared the SRO ceramic target. X.Y., Z.L., J.L., X.L., and C.T. performed the synchrotron x-ray diffraction, electrical transport, and XPS measurements. X.Y. and J.W. carried out the superconducting quantum interference device measurement. L.S., P.J., Z.Z., and K.H. performed the theoretical calculations. I.M. and J.L. carried out the atomic force microscopy and MFM measurements. Q.Z. and L.G. performed STEM measurement. Z.L. performed the RSM

measurement. J.Z., C.-W.N., Z.Z., and W.M. were involved in the discussion and revision of the paper. All authors were involved in the analysis of the experimental and theoretical results.

[1] F. Matsukura, Y. Tokura, and H. Ohno, Nat. Nanotechnol. **10**, 209 (2015).
[2] S. Dong, J.-M. Liu, S.-W. Cheong, and Z. Ren, Adv. Phys. **64**, 519 (2015).
[3] N. A. Spaldin and R. Ramesh, Nat. Mater. **18**, 203 (2019).
[4] N. A. Spaldin, Proc. R. Soc. A **476**, 20190542 (2020).
[5] V. Garcia, M. Bibes, L. Bocher, S. Valencia, F. Kronast, A. Crassous, X. Moya, S. Enouz-Vedrenne, A. Gloter, D. Imhoff, C. Deranlot, N. D. Mathur, S. Fusil, K. Bouzehouane, and A. Barthélémy, Science **327**, 1106 (2010).
[6] J. T. Heron, M. Trassin, K. Ashraf, M. Gajek, Q. He, S. Y. Yang, D. E. Nikonov, Y. H. Chu, S. Salahuddin, and R. Ramesh, Phys. Rev. Lett. **107**, 217202 (2011).
[7] T. H. Lahtinen, J. O. Tuomi, and S. van Dijken, Adv. Mater. **23**, 3187 (2011).
[8] P. J. Ryan, J. W. Kim, T. Birol, P. Thompson, J. H. Lee, X. Ke, P. S. Normile, E. Karapetrova, P. Schiffer, S. D. Brown, C. J. Fennie, and D. G. Schlom, Nat. Commun. **4**, 1334 (2013).
[9] L. T. Chang, C. Y. Wang, J. Tang, T. Nie, W. Jiang, C. P. Chu, S. Arafin, L. He, M. Afsal, L. J. Chen, and K. L. Wang, Nano Lett. **14**, 1823 (2014).
[10] Y. S. Oh, S. Artyukhin, J. J. Yang, V. Zapf, J. W. Kim, D. Vanderbilt, and S. W. Cheong, Nat. Commun. **5**, 3201 (2014).
[11] K. J. A. Franke, B. Van de Wiele, Y. Shirahata, S. J. Hämäläinen, T. Taniyama, and S. van Dijken, Phys. Rev. X **5**, 011010 (2015).
[12] M. Ziese, I. Vrejoiu, E. Pippel, P. Esquinazi, D. Hesse, C. Etz, J. Henk, A. Ernst, I. V. Maznichenko, W. Hergert, and I. Mertig, Phys. Rev. Lett. **104**, 167203 (2010).
[13] M. Verissimo-Alves, P. Garcia-Fernandez, D. I. Bilc, P. Ghosez, and J. Junquera, Phys. Rev. Lett. **108**, 107003 (2012).
[14] A. J. Grutter, B. J. Kirby, M. T. Gray, C. L. Flint, U. S. Alaan, Y. Suzuki, and J. A. Borchers, Phys. Rev. Lett. **115**, 047601 (2015).
[15] L. Si, Z. Zhong, J. M. Tomczak, and K. Held, Phys. Rev. B **92**, 041108(R) (2015).
[16] H. T. Dang, J. Mravlje, A. Georges, and A. J. Millis, Phys. Rev. B **91**, 195149 (2015).
[17] M. Kim and B. I. Min, Phys. Rev. B **91**, 205116 (2015).
[18] D. Kan, R. Aso, R. Sato, M. Haruta, H. Kurata, and Y. Shimakawa, Nat. Mater. **15**, 432 (2016).
[19] V. Granata, L. Capogna, F. Forte, M.-B. Lepetit, R. Fittipaldi, A. Stunault, M. Cuoco, and A. Vecchione, Phys. Rev. B **93**, 115128 (2016).
[20] H. Boschker, T. Harada, T. Asaba, R. Ashoori, A. V. Boris, H. Hilgenkamp, C. R. Hughes, M. E. Holtz, L. Li, D. A. Muller, H. Nair, P. Reith, X. Renshaw Wang, D. G. Schlom, A. Soukiassian, and J. Mannhart, Phys. Rev. X **9**, 011027 (2019).
[21] L. Klein, J. S. Dodge, C. H. Ahn, G. J. Snyder, T. H. Geballe, M. R. Beasley, and A. Kapitulnik, Phys. Rev. Lett. **77**, 2774 (1996).
[22] A. J. Grutter, F. J. Wong, E. Arenholz, A. Vailionis, and Y. Suzuki, Phys. Rev. B **85**, 134429 (2012).
[23] X. K. Ning, Z. J. Wang, and Z. D. Zhang, J. Appl. Phys. **117**, 093907 (2015).
[24] M. Gu, K. Wang, Y. Wang, Q. Xie, H. Cai, G.-P. Zhang, and X. Wu, npj Quantum Mater. **1**, 16011 (2016).
[25] J. Matsuno, N. Ogawa, K. Yasuda, F. Kagawa, W. Koshibae, N. Nagaosa, Y. Tokura, and M. Kawasaki, Sci. Adv. **2**, e1600304 (2016).
[26] L. Wang, Q. Feng, Y. Kim, R. Kim, K. H. Lee, S. D. Pollard, Y. J. Shin, H. Zhou, W. Peng, D. Lee, W. Meng, H. Yang, J. H. Han, M. Kim, Q. Lu, and T. W. Noh, Nat. Mater. **17**, 1087 (2018).
[27] Y. Ohuchi, J. Matsuno, N. Ogawa, Y. Kozuka, M. Uchida, Y. Tokura, and M. Kawasaki, Nat. Commun. **9**, 213 (2018).
[28] Q. Qin, L. Liu, W. Lin, X. Shu, Q. Xie, Z. Lim, C. Li, S. He, G. M. Chow, and J. Chen, Adv. Mater. **31**, 1807008 (2019).
[29] D. Toyota, I. Ohkubo, H. Kumigashira, M. Oshima, T. Ohnishi, M. Lippmaa, M. Takizawa, A. Fujimori, K. Ono, M. Kawasaki, and H. Koinuma, Appl. Phys. Lett. **87**, 162508 (2005).
[30] S. Kang, Y. Tseng, B. H. Kim, S. Yun, B. Sohn, B. Kim, D. McNally, E. Paris, C. H. Kim, C. Kim, T. W. Noh, S. Ishihara, T. Schmitt, and J.-G. Park, Phys. Rev. B **99**, 045113 (2019).
[31] H. G. Lee, L. Wang, L. Si, X. He, D. G. Porter, J. R. Kim, E. K. Ko, J. Kim, S. M. Park, B. Kim, A. T. S. Wee, A. Bombardi, Z. Zhong, and T. W. Noh, Adv. Mater. **32**, 1905815 (2020).
[32] J. M. Rondinelli, M. Stengel, and N. A. Spaldin, Nat. Nanotechnol. **3**, 46 (2008).
[33] L. Si, O. Janson, G. Li, Z. Zhong, Z. Liao, G. Koster, and K. Held, Phys. Rev. Lett. **119**, 026402 (2017).
[34] W. Shockley, Bell Syst. Tech. J. **28**, 435 (1949).
[35] E. J. Guo, Y. Liu, C. Sohn, R. D. Desautels, A. Herklotz, Z. Liao, J. Nichols, J. W. Freeland, M. R. Fitzsimmons, and H. N. Lee, Adv. Mater. **30**, 1705904 (2018).
[36] See Supplemental Material at http://link.aps.org/supplemental/10.1103/PhysRevB.101.214401 for additional data and details on the experiments and data analysis, which include Refs. [37–39].
[37] W. Lu, P. Yang, W. D. Song, G. M. Chow, and J. S. Chen, Phys. Rev. B **88**, 214115 (2013).
[38] Z. T. Xu, K. J. Jin, L. Gu, Y. L. Jin, C. Ge, C. Wang, H. Z. Guo, H. B. Lu, R. Q. Zhao, and G. Z. Yang, Small **8**, 1279 (2012).
[39] J. B. Gilbert, M. F. Rubner, and R. E. Cohen, Proc. Natl. Acad. Sci. USA **110**, 6651 (2013).
[40] M. E. Fisher and J. S. Langer, Phys. Rev. Lett. **20**, 665 (1968).
[41] M. Ziese, I. Vrejoiu, and D. Hesse, Phys. Rev. B **81**, 184418 (2010).
[42] G. Koster, L. Klein, W. Siemons, G. Rijnders, J. S. Dodge, C.-B. Eom, D. H. A. Blank, and M. R. Beasley, Rev. Mod. Phys. **84**, 253 (2012).
[43] A. Kanbayasi, J. Phys. Soc. Jpn. **41**, 1876 (1976).
[44] P. B. Allen, H. Berger, O. Chauvet, L. Forro, T. Jarlborg, A. Junod, B. Revaz, and G. Santi, Phys. Rev. B **53**, 4393 (1996).
[45] D. J. Singh, J. Appl. Phys. **79**, 4818 (1996).
[46] S. N. Bushmeleva, V. Y. Pomjakushin, E. V. Pomjakushina, D.

V. Sheptyakov, and A. M. Balagurov, J. Magn. Magn. Mater. **305**, 491 (2006).
[47] N. Pavlenko, T. Kopp, E. Y. Tsymbal, J. Mannhart, and G. A. Sawatzky, Phys. Rev. B **86**, 064431 (2012).
[48] M. Mlynarczyk, K. Szot, A. Petraru, U. Poppe, U. Breuer, R. Waser, and K. Tomala, J. Appl. Phys. **101**, 023701 (2007).
[49] See Supplemental Material at http://link.aps.org/supplemental/10.1103/PhysRevB.101.214401 for the calculational details and additional data, which include Refs. [50–57].
[50] P. C. Hohenberg and W. Kohn, Phys. Rev. **136**, B864 (1964).
[51] W. Kohn and L. J. Sham, Phys. Rev. **140**, A1133 (1965).
[52] J. P. Perdew, K. Burke, and M. Ernzerhof, Phys. Rev. Lett. **77**, 3865 (1996).
[53] G. Kresse and D. Joubert, Phys. Rev. B **59**, 1758 (1999).
[54] G. Kresse and J. Furthmüller, Comput. Mater. Sci. **6**, 15 (1996).
[55] P. Blaha, K. Schwarz, G. K. H. Madsen, D. Kvasnicka, and J. Luitz, *WIEN2K: An Augmented Plane Wave Plus Local Orbitals Program for Calculating Crystal Properties* (TU Wien, Austria, 2001).
[56] V. I. Anisimov, J. Zaanen, and O. K. Andersen, Phys. Rev. B **44**, 943 (1991).
[57] S. L. Dudarev, G. A. Botton, S. Y. Savrasov, C. J. Humphreys, and A. P. Sutton, Phys. Rev. B **57**, 1505 (1998).
[58] A. Walsh, C. R. A. Catlow, A. G. H. Smith, A. A. Sokol, and S. M. Woodley, Phys. Rev. B **83**, 220301(R) (2011).
[59] T. Leisegang, H. Stocker, A. A. Levin, T. Weissbach, M. Zschornak, E. Gutmann, K. Rickers, S. Gemming, and D. C. Meyer, Phys. Rev. Lett. **102**, 087601 (2009).